Extracting Noise Producing Coherent Structures in Cylinder Flows from TR PIV Data

Robin Prinja, Florent Margnat, Peter Jordan

Extracting Noise Producing Coherent Structures in Cylinder Flows from TR PIV Data

Robin Prinja*, Florent Margnat† and Peter Jordan‡
Département Fluides, Thermique et Combustion, Institut Pprime, Université de Poitiers, Poitiers, 86000

For a subcritical flow around a circular cylinder with a turbulent wake, Time resolved Particle image velocimetry (TR PIV) experiments have been performed to study and extract the large scale flow structures that lead to far-field noise. This has been done by decomposing the flow velocity fluctuation fields into their frequency and spanwise wavenumber modes and a low-order system has been found which can be used to develop noise prediction models. Then by using the far-field acoustic measurements, which were synchronised with the TR PIV, acoustic contribution of individual spanwise wavenumber mode is evaluated at the tonal frequency. Also, the global features of the flow have been characterized by presenting the time-averaged mean flow velocities and turbulent statistics.

I. Introduction

Flow over a cylinder is widely studied as a canonical problem for bluff body flow and its aeroacoustics (such as [1–5]). The applications for such problem can be found in various subjects such as aiframe noise where landing gear and high-lift devices are primary noise sources.

High-fidelity simulations such as Direct Numerical Simulation (DNS) or Large Eddy Simulation (LES) have been used in the past (for instance, see [2, 6]) to study the flow around the cylinders and in the wake region. They are significant tools to have an in-depth understanding of the key hydrodynamic motions. For low Reynolds number, Re flows, they can even be used for noise prediction (see [7] for instance) but for high-Re, such simulations can be very expensive for long span cylindrical bodies because of high length scale difference in the turbulent motions and acoustic perturbations. For this, hybrid methods are often used that consists of solving the near-field hydrodynamics with a high-fidelity simulation and then using an acoustic analogy to predict the far-field noise (for instance, see [8]). But in such hybrid methods also, an expensive near-field simulation is required, and also there is less understanding of the parts of the flow fluctuations that actually contribute to the far-field noise.

In the present work, we work towards developing the physics-based noise prediction models that are of low-order and inexpensive. To develop such models, we analyse the Time resolved Particle image velocimetry (TR PIV) experimental data for the flow over a circular cylinder, so as to extract the primary noise producing components of the flow fluctuations, which are the large scale coherent structures. We do this by decomposing the velocity fluctuation field into the frequency-wavenumber modes. Also, by using the synchronised far-field acoustic measurements, we investigate the acoustic efficiency of each of these modes. Also, we present the time-averaged mean velocity fields and turbulent statistics to characterize the flow. The amplitudes of the coherent structures and time-averaged mean flow obtained in the present work are also used in the noise prediction model that we present in a parallel investigation in the same conference [9].

The primary feature of the flow over a cylinder is a tonal noise generated by the periodic flow distortions associated with the interaction of wakes, the phenomenon which is popularly known as von Kármán vortex street. This phenomenon can be seen as a stream of alternately rotating vortices that perseveres till many diameters downstream. First studied by Strouhal [10], the frequency of tonal noise from this vortex shedding is given as,

$$f = St \times \frac{U_\infty}{d}, \tag{1}$$

where St is the Strouhal number, U_∞ is the free-stream velocity and d is the cylinder diameter. This vortex shedding based tonal noise feature is inherent in the wake flows ranging from low-Re flows to high-Re turbulent flows [11].

*Graduate Student, robin.prinja@univ-poitiers.fr
†Assistant Professor, florent.margnat@univ-poitiers.fr
‡Research Director, peter.jordan@univ-poitiers.fr

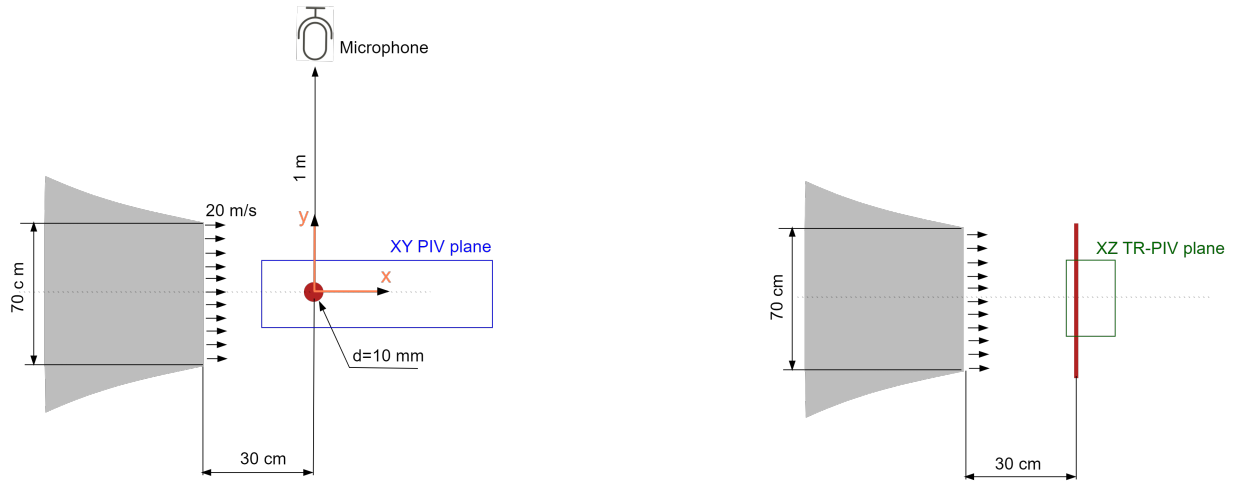

Fig. 1 Schematic diagram for $Re = 13000$ flow over a circular cylinder (not to scale). Front view (at left) and top view (at right) are shown.

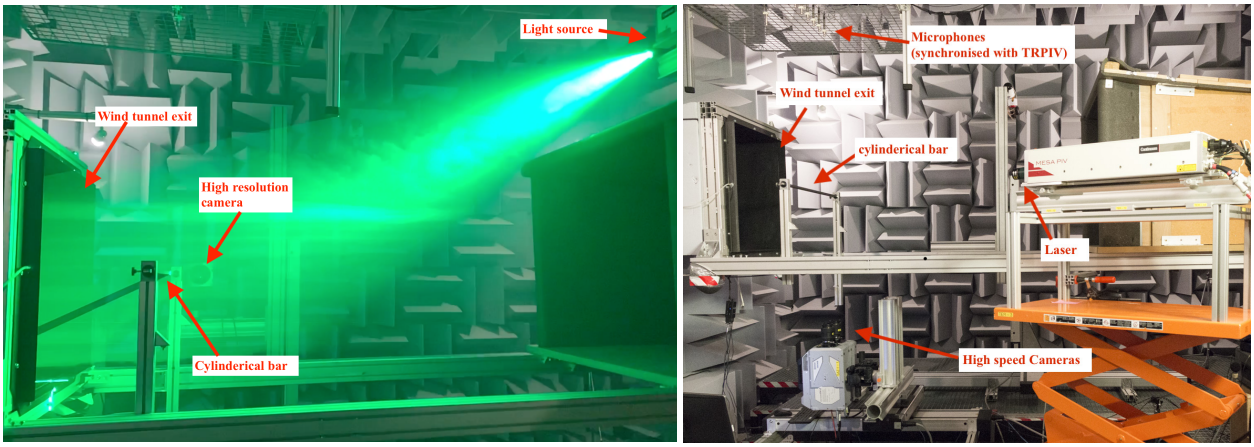

(a) XY PIV campaign **(b) XZ TR-PIV campaign**

Fig. 2 PIV experiments setup at the anechoic wind-tunnel BETI of the Pprime Institute, at Poitiers, France.

In the present work, we present the study of the flow around a circular cylinder for Reynolds number, $Re = U_\infty d/\nu = 13000$, where ν is the dynamic viscosity.

The paper is organised as follows. Section II presents the details of the flow configuration and the employed experimental setup. In section III, the time-averaged mean flow characteristics in the XY plane such as velocity fields and turbulent statistics are presented. Section IV presents the flow dynamics in the XZ plane, where the fluctuation field is decomposed into its frequency-wavenumber modes to extract the large scale coherent structures behind the noise emissions. Also, the acoustic efficiency of each spanwise mode is evaluated by calculating their coherence with the far-field pressure fluctuations.

II. Flow configuration & experimental setup

The sketch of overall flow configuration can be seen in the Fig. 1. The flow consists of $U_\infty = 20$m/s airflow over a circular cylinder ($d = 10$mm) at NTP conditions exiting from the nozzle section 70×70cm with the turbulent intensity of 0.5% at 30cm downstream, where the cylinder is mounted. This corresponds to $Re = 13000$ and the flow consists of features such as turbulent wake, and noise production and propagation to the far-field.

For the present case (Fig. 1), the origin of coordinate system is kept at the cylinder center. The wind-tunnel jet is

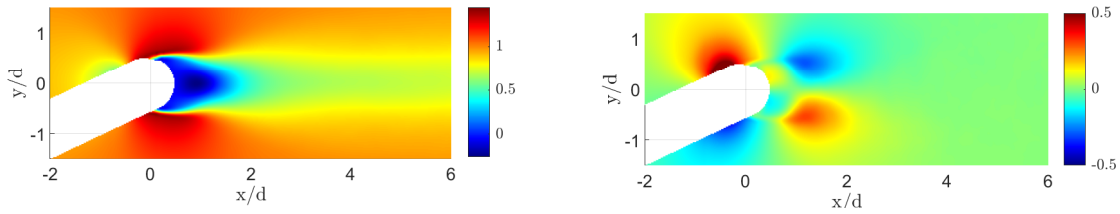

(a) Streamwise velocity, U/U_∞ **(b) Transverse velocity, V/U_∞**

Fig. 3 Time-averaged mean flow.

along $x-$axis and cylinder's span is along $z-$axis. Two set of PIV experiments were performed: (i) PIV in the mid-span XY plane (domain shown in blue in Fig. 1) to measure the time-averaged mean velocity field and turbulent statistics in the XY plane; (ii) TR-PIV in the XZ plane at $y/d = -1$ (domain shown in green in Fig. 1) to study and characterise the velocity fluctuation field. For the XZ TRPIV campaign, a microphone (synchronised with TRPIV) is also kept at $x/d = 0, y/d = 100, z/d = 0$ to record the far-field pressure fluctuations.

All the experiments have been performed at the anechoic wind-tunnel BETI of Pprime Institute, at Poitiers, France. The photos of the experiment setup are shown in Fig. 2 for the two PIV campaigns. XY PIV experiment setup consists of a high resolution camera and light source kept at top-right corner. XZ TRPIV experiment setup consists of two high-speed cameras placed directly under the cylinder, and focused on the XZ plane $y/d = 1$, light source on the right and a microphone kept at $y/d = 100$ (in sync with the XZ TRPIV).

III. Flow dynamics in XY plane

The time-averaged mean flow velocity and turbulent statistics in the XY plane are presented in this section. For the present work, this has been obtained by PIV system setup in the mid-span XY plane as shown in Figs. 1(left) and 2a. The experiments setup consists of: (i) High resolution camera *Phantom VEO 4K 990L* (4096×2304 pixels), and the images were taken with a sampling frequency of 100Hz . (ii) Laser Continuum Terra PIV (2 x 30 mJ), synchronised with the camera, was used to illuminate periodically the seeding; the time-delay between two consecutive laser illuminations was kept as 10μs so as to capture even the important fast scale motions.

For data analysis, LaVision Davis 10 software was used to get the velocity field and the steady-state statistics. The interrogation window size was kept as 32×32 pixels and 75% overlap. This yielded the PIV domain of [$-11 < x/d < 11$, $-2 < y/d < 2$] with the spatial resolution of $\Delta x/d = \Delta y/d = 0.0235$; and 6000 time-steps were recorded to ensure the the convergence of mean statistics.

The time-averaged mean streamwise velocity (U) and transverse velocity (V) from the Davis are shown in the Fig. 3. In Fig. 3, we see that the shear-layers at the top and bottom sides of the cylinder slowly merge together creating a wake that extends to several diameters downstream. Some flow features can be better understood by looking at the mean velocity vectors as in Fig. 4 where the recirculation region behind the cylinder is clearly visible, that consists of two oppositely rotating vortices centred at ($x/d \approx 0.8, y/d \approx \pm 0.25$). There is a stagnation point at $x/d = 1.3$ at $y = 0$ axis. The mean vorticity ($\zeta_z = \nabla \times \mathbf{U}$) is shown in Fig. 5 which tells the same story.

The turbulent steady-state statistics are shown in Fig. 6, where Reynolds stresses ($R_{xx} = \rho\overline{u^2}$, $R_{yy} = \rho\overline{v^2}$ and $R_{xy} = \rho\overline{uv}$) and turbulent kinetic energy, $TKE = \rho(\overline{u^2} + \overline{v^2})/2$ are shown (here, u and v are the streamwise and transverse velocity fluctuations respectively, and ρ is the flow density). R_{xx} peaks in the shear layer regions while R_{yy} peaks at the centerline ($y = 0$) around $x/d = 1.4$ which is just downstream of the stagnation point ($x/d = 1.3$).

The centreline profiles for some of the turbulent statistics (U, R_{xx} and R_{yy}) are shown in Fig. 7a. The mean streamwise velocity is also compared withe the LES done by Prsic et al. [12] and a good agreement has been found. The stagnation point for U is around $x/d = 1.3$ at the centerline, near which R_{xx} and TKE peak also. At $x/d = 1.3$ (the stagnation point), y-profiles for mean velocities and Reynolds stresses are shown in Fig. 7b.

IV. Extracting the dominant fluctuating structures from TR PIV in XZ plane

In this section, the velocity fluctuation fields are studied and the large-scale dominant coherent structures are extracted which are the building blocks for noise prediction models. For this, high speed TR PIV system in the XZ

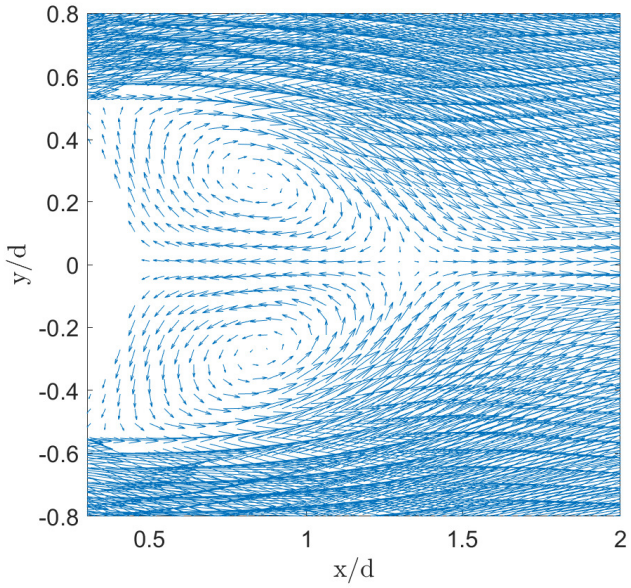

Fig. 4 Mean flow velocity vectors.

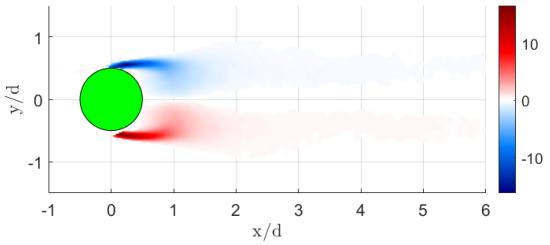

Fig. 5 Mean vorticity, $\zeta_z \times d/U_\infty$.

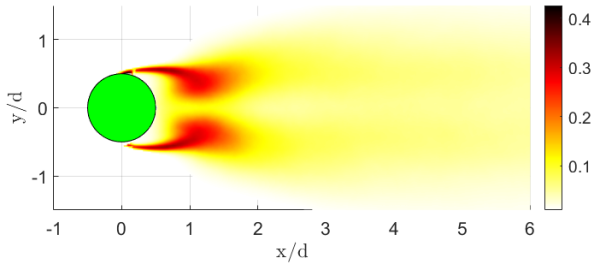

(a) R_{xx}/U_∞^2

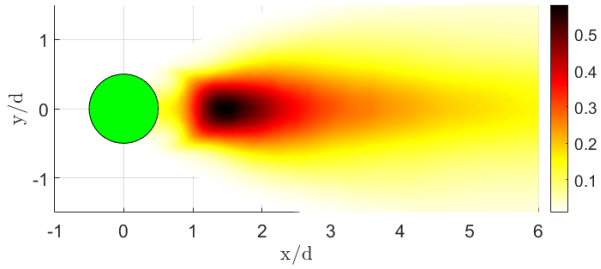

(b) R_{yy}/U_∞^2

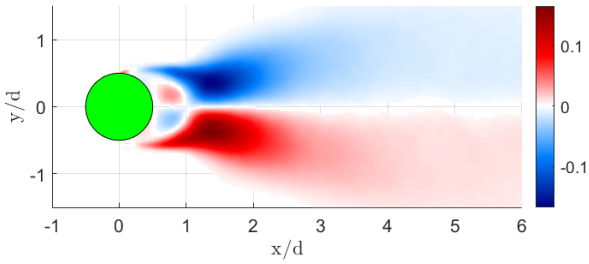

(c) R_{xy}/U_∞^2

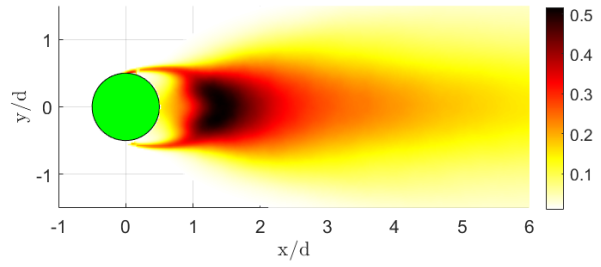

(d) TKE/U_∞^2

Fig. 6 Colormaps for turbulent statistics.

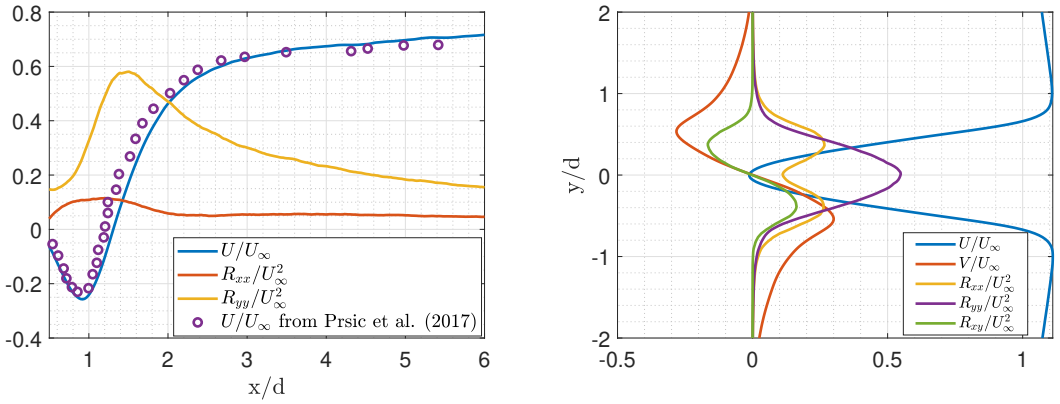

(a) $X-$**profiles for** $y/d = 0$ **(b)** $Y-$**profiles for** $x/d = 1.3$

Fig. 7 $X-$ **and** $y-$ **profiles for mean velocities and some turbulent statistics.**

plane at $y/d = -1$ has been setup as shown in the Figs. 1(right) and 2b. The experiments setup consists of: (i) Two high speed cameras *Photron Fastcam SA-Z* (1024 × 1024 pixels) placed side by side taking images at the sampling frequency of 20kHz; (ii) Continuum Mesa PIV (2 x 9 mJ), synchronised with the camera; the time-delay between two consecutive laser illuminations was kept as 20μs; and (iii) A microphone (synchronised with TR PIV) kept at $x/d = 0, y/d = 100, z/d = 0$ to record the far-field pressure fluctuations.

Velocity fields from PIV images were obtained from LaVision Davis 10 software with an interrogation window size of 16×16 pixels and 75% overlap. Finally, we have 22000 time-steps of velocity field with sampling frequency of $F_s = 10$kHz in the spatial domain $[-2 < x/d < 14, -15 < z/d < 15\ ]$, with the spatial resolution of $\Delta x/d = \Delta z/d = 0.1263$. The spanwise homogeneity and convergence of the turbulent statistics were assured.

The mean streamwise velocity field (U) and Reynolds stress (R_{xx}) are shown in the Fig. 8 which look fairly homogeneous in the spanwise direction, and their $x-$profiles match with the ones from XY PIV (Figs. 3 and 6a).

The fluctuation time-series ($u(x, z, t)$) was split into 108 realizations, where each realization contains 800 snapshots and overlap of 75%. It was then decomposed into Fourier modes in the frequency domain using Eq. 2. This leads to frequency resolution of $\Delta St = \Delta f d/U_\infty = 0.006$.

$$\mathbf{u}(x, z, t) = \sum_{\omega} \hat{\mathbf{u}}_\omega(x, z)\ e^{i\omega t}, \tag{2}$$

where ω is the angular frequency of the fourier modes.

A. Decomposition of fluctuation field CSD into its spanwise fourier modes

Here we aim to extract the dominant coherent structures in the fluctuation field, these structures remains correlated over large length and time scales. These are the ones that drive vortex shedding in the hydrodynamic near-field and acoustics tones in the far-field.

An instantaneous snapshot for the streamwise velocity fluctuation is shown in Fig. 9a. Large scale coherent structures can be observed hinting the system to be of low order. For the mid-span axis, $z/d = 0$, the power spectral density (PSD) colormap for streamwise-velocity fluctuations is shown in Fig. 9b. Figure 9b shows that there exists a single frequency, $St \approx 0.2$ that corresponds to the VS frequency, which is dominating the fluctuation field and this was found to be same for all the spanwise locations.

Then, we calculate the cross spectral density (CSD) of the streamwise velocity fluctuation field as,

$$S_{z_0 z, \omega}(x) = \hat{u}_\omega(x, z_0)\, \hat{u}^*_\omega(x, z), \tag{3}$$

where $z_0 = 0$ is chosen as the reference position and * represents the complex conjugate. The bandlimited power spectrum (BPS) of CSD for $St = 0.2 \pm 2.5\%$ is shown in Fig. 9c. The strong magnitudes of the CSD even for $z/d \approx 5$ signifies the large spanwise length scale of the coherent structures.

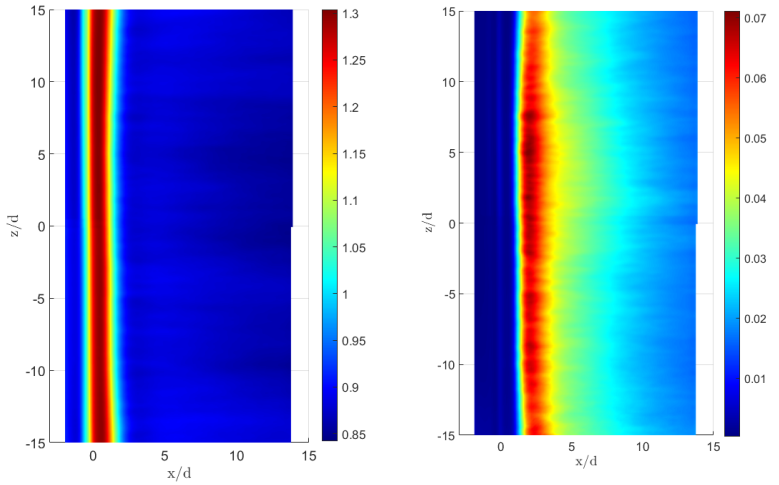

(a) U/U_∞ **(b)** R_{xx}/U_∞^2

Fig. 8 Mean streamwise velocity U and Reynolds stress, R_{xx} at $y/d = -1$.

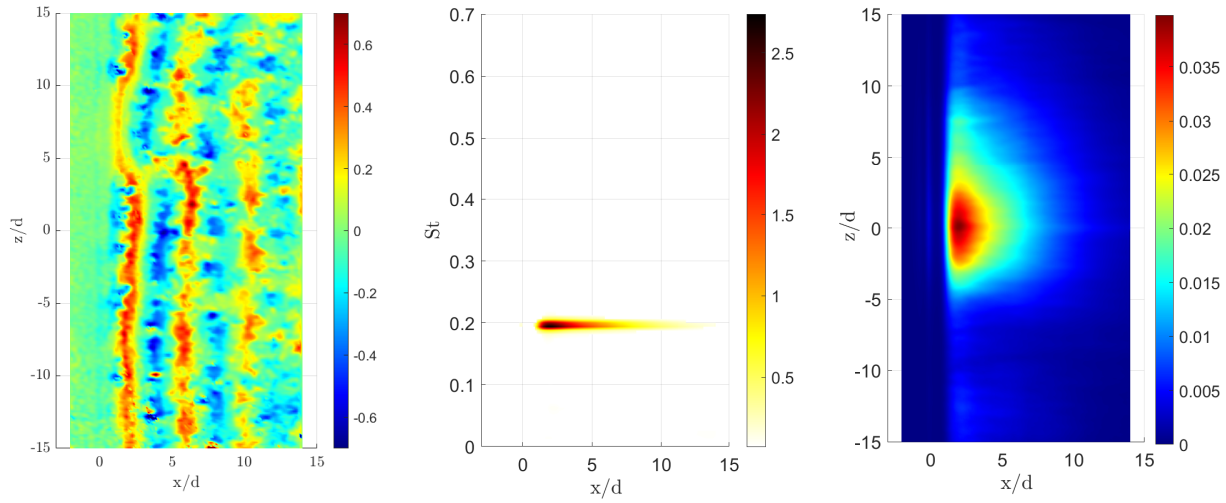

(a) u/U_∞**, at a time-instant** **(b)** $\hat{u}\hat{u}/U_\infty^2$ **PSD at** $z/d = 0$**.** **(c)** $S_{z_0 z}/U_\infty^2$ **BPS for** $St = 0.2 \pm 2.5\%$

Fig. 9 XZ TRPIV at $y/d = -1$: streamwise velocity fluctuations.

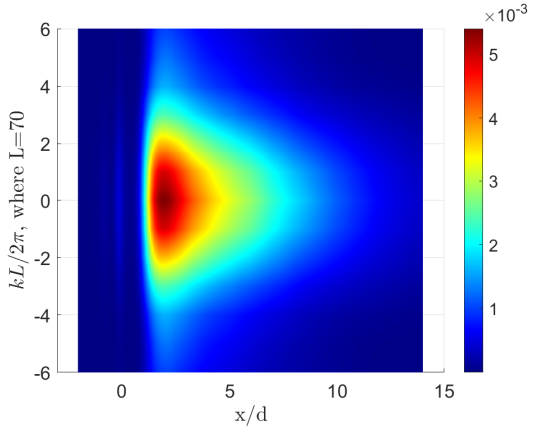

Fig. 10 XZ TR PIV at $y/d = -1$: $\tilde{S}/U_\infty^2$ BPS for $St = 0.2 \pm 2.5\%$

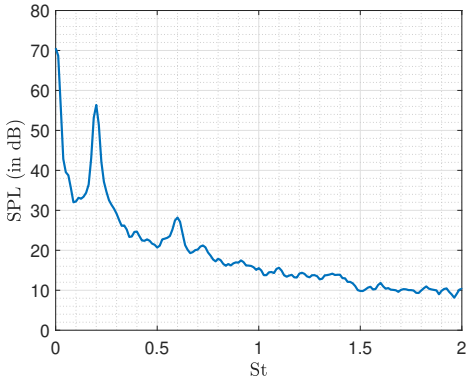

Fig. 11 Farfield acoustic measurements: SPL at $x/d = 0, y/d = 100$.

The CSD is then decomposed into its spanwise Fourier modes as,

$$S_{z_0 z,\omega}(x) = \sum_{k=-\infty}^{\infty} \tilde{S}_{k,\omega}(x)\ e^{ikz}, \tag{4}$$

where $\tilde{S}_{k,\omega}$ can be evaluated from CSD as,

$$\tilde{S}_{k,\omega}(x) = \frac{1}{L} \sum_{z=-L/2}^{L/2} S_{z_0 z,\omega}(x)\ e^{-ikz}\ \Delta z, \tag{5}$$

where $L = 70d$ is the cylinder's spanwise length (defined as the periodic length of the system) and Δz is the spanwise resolution. Its BPS for $St = 0.2 \pm 2.5\%$, is shown in Fig. 10 which peaks near $x/d \approx 2$ which is same as the peak R_{xx} location. Also, it shows the low-rank behaviour i.e. only $\mid k \mid \leq 5$ spanwise wavenumbers are important.

B. Acoustic contribution of individual spanwise modes

We aim to identify here the spanwise fourier modes, for streamwise velocity fluctuations (u), which contribute most in the far-field noise. We decompose u into its spanwise fourier modes and calculate the acoustic efficiency of each of them by computing their coherence with the pressure fluctuations at the microphone kept in the far-field.

1. Far-field pressure fluctuations in frequency space

The pressure fluctuations, p, were recorded at $x/d = 0, y/d = 100$ with microphone with a sampling frequency of 50kHz and acquisition time of 6s. Using the TR PIV synchronisation information, the pressure fluctuations were extracted for the same time-instants as u fluctuations from TR PIV. Using same fast Fourier transform (FFT) parameters as for u fluctuations, p was decomposed into its Fourier modes as,

$$p(t) = \sum_{\omega} \hat{p}_\omega\ e^{i\omega t}. \tag{6}$$

Figure 11 shows the Sound Pressure Level (SPL) spectra (with reference sound pressure, $p_0 = 20\mu$Pa) at the microphone location. There is a peak at $St = 0.2$ that corresponds to the vortex shedding mode, also there is another minor peak at its third harmonic. Also, there is a fluctuation energy in the low-frequency region ($0 < f < 50$Hz) which are below the anechoic frequency cutoff of the wind-tunnel.

2. Streamwise velocity fluctuations in frequency-wavenumber space

The streamwise velocity fluctuation, $\hat{u}$ from Eq. 2 was decomposed into its spanwise Fourier modes as,

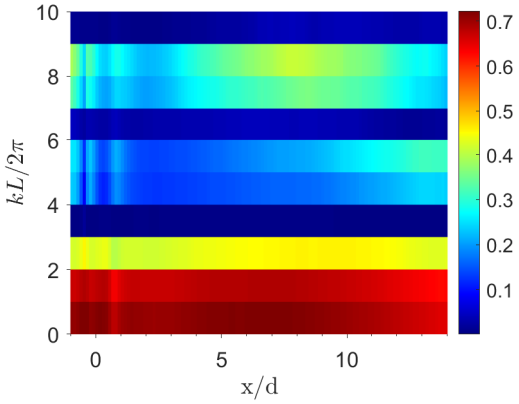

Fig. 12 Coherence, γ^2, for $St = 0.2$.

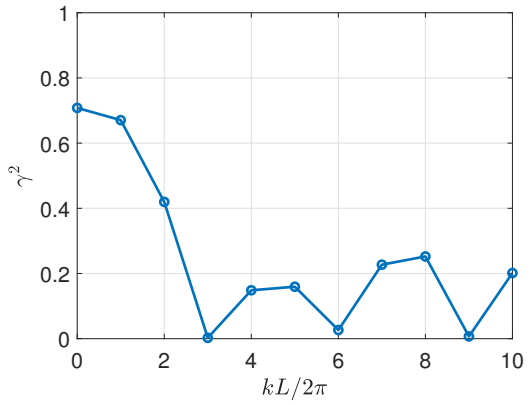

Fig. 13 Coherence, γ^2, for $St = 0.2$ at $x/d = 1.3$.

$$\tilde{u}_{k,\omega}(x) = \frac{1}{L} \sum_{z=-L/2}^{L/2} \hat{u}_{\omega}(x,z)\ e^{-ikz}\ \Delta z. \tag{7}$$

3. Acoustic contribution

The contribution of each spanwise modes in the far-field noise is then evaluated by computing their coherence with the far-field pressure fluctuations as,

$$\gamma^2_{k,\omega}(x) = \frac{\left|\hat{\mathbf{p}}_{\omega} \cdot \tilde{\mathbf{u}}^*_{k,\omega}(x)\right|^2}{\left|\hat{\mathbf{p}}_{\omega} \cdot \hat{\mathbf{p}}^*_{\omega}\right| \left|\tilde{\mathbf{u}}_{k,\omega}(x) \cdot \tilde{\mathbf{u}}^*_{k,\omega}(x)\right|} \tag{8}$$

where $\hat{\mathbf{p}}$ represents the vector description of $\hat{p}$ from 215 FFT realizations, $\tilde{\mathbf{u}}$ represents the the vector description of $\tilde{u}$ from 215 FFT realizations, and $\cdot$ represents the dot product.

For $St = 0.2$, the acoustic contribution of each spanwise mode is shown in Fig. 12, which is seen to be independent of x position. Figure 13 shows the same parameter, but at $x/d = 1.3$, to have a clearer visual. It can be seen than for all the spanwise fourier mode $k > 2$, the acoustic efficiency is very low ($\gamma^2 < 0.2$), which shows that the dominant fluctuation field behind noise generation is a low rank system.

V. Conclusion

The flow over a circular cylinder from TR PIV experiments has been analysed. The time-averaged mean statistics and velocity fluctuation field were investigated in order to identify and extract the large-scale coherent structures that lead to far-field tonal noise. It was found that in the frequency-wavenumber space, a very few number of modes at vortex shedding frequency are required to represent the velocity fluctuation cross spectral density. These modes can be used to develop low-rank noise prediction models. Using the far-field acoustic recordings, synchronised with TR PIV, the acoustic contribution of each of the velocity fluctuation spanwise modes were calculated and it was found that only $k \leq 2$ spanwise wavenumber modes were actually contributing to the far-field noise.

References

[1] Berger, E., and Wille, R., "Periodic flow phenomena," *Annual Review of Fluid Mechanics*, Vol. 4, No. 1, 1972, pp. 313–340.

[2] Kravchenko, A. G., and Moin, P., "Numerical studies of flow over a circular cylinder at Re D= 3900," *Physics of fluids*, Vol. 12, No. 2, 2000, pp. 403–417.

[3] Bloor, M. S., "The transition to turbulence in the wake of a circular cylinder," *Journal of Fluid Mechanics*, Vol. 19, No. 2, 1964, pp. 290–304.

[4] Travin, A., Shur, M., Strelets, M., and Spalart, P., "Detached-eddy simulations past a circular cylinder," *Flow, turbulence and combustion*, Vol. 63, No. 1, 2000, pp. 293–313.

[5] Norberg, C., "Effects of Reynolds number and a low-intensity freestream turbulence on the flow around a circular cylinder," *Chalmers University, Goteborg, Sweden, Technological Publications*, Vol. 87, No. 2, 1987, pp. 1–55.

[6] Trias, F., Gorobets, A., and Oliva, A., "Turbulent flow around a square cylinder at Reynolds number 22,000: A DNS study," *Computers & Fluids*, Vol. 123, 2015, pp. 87–98.

[7] Inoue, O., and Hatakeyama, N., "Sound generation by a two-dimensional circular cylinder in a uniform flow," *Journal of Fluid Mechanics*, Vol. 471, 2002, pp. 285–314.

[8] Pérot, F., Gloerfelt, X., Bailly, C., Auger, J.-M., and Giardi, H., "Numerical prediction of the noise radiated by a cylinder," *9th AIAA/CEAS aeroacoustics conference and exhibit*, 2003, p. 3240.

[9] Prinja, R., Jordan, P., and Margnat, F., "Modeling aeolian tones by global stability modes," *28th AIAA/CEAS Aeroacoustics Conference*, 2022.

[10] Strouhal, V., *Über eine besondere Art der Tonerregung*, Stahel, 1878.

[11] Williamson, C. H., "Vortex dynamics in the cylinder wake," *Annual review of fluid mechanics*, Vol. 28, No. 1, 1996, pp. 477–539.

[12] Prsic, M. A., Ong, M. C., Pettersen, B., and Myrhaug, D., "Large Eddy Simulations of flow around a smooth circular cylinder in a uniform current in the subcritical flow regime," *Ocean Engineering*, Vol. 77, 2014, pp. 61–73.